Marine Micropaleontology

Integrated calcareous nannofossil and magnetostratigraphic record of ODP Site 709: middle Eocene to late Oligocene paleoclimate and paleoceanography of the Equatorial Indian Ocean

--Manuscript Draft--

Manuscript Number:	MARMIC-D-21-00006
Article Type:	Research Paper
Keywords:	Calcareous nannofossils; Eocene; Oligocene; Biomagnetostratigraphy; Paleoceanography; ODP Site 709
Corresponding Author:	GIULIANA VILLA University of Parma: Universita degli Studi di Parma ITALY
First Author:	GIULIANA VILLA
Order of Authors:	GIULIANA VILLA
	Fabio Florindo
	Davide Persico
	Pontus Lurcock
	Ana Paula de Martini
	Luigi Jovane
	Chiara Fioroni
Manuscript Region of Origin:	Europe
Abstract:	We investigate the calcareous nannofossil biostratigraphy and magnetostratigraphy of middle Eocene – lower Oligocene sediments from ODP Hole 709 C.
Suggested Reviewers:	• Shijun Jiang Jinan University, Guangzhou, China sjiang@jnu.edu.cn
	Carlotta Cappelli Universita Padova DG: Universita degli studi di Padova Dipartimento di Geoscienze carlotta.cappelli@unipd.it
	Gary Wilson g.wilson@gmns.cri.nz
	Andrew Roberts Australian National University College of Science: Australian National University andrew.roberts@anu.edu.au

Cover letter

Dear Editor,

Here is a manuscript by myself and co-authors entitled "***Integrated calcareous nannofossil and magnetostratigraphic record of ODP Site 709: middle Eocene to late Oligocene paleoclimate and paleoceanography of the Equatorial Indian Ocean***
In this paper we provide a new paleoceanographic interpretation for the Middle Eocene-Late Oligocene interval of the Equatorial Indian Ocean, by means of calcareous nannofossil assemblage and magnetostratigraphy.
Given the importance of the paleoclimatic and paleoceanographic implications of the time interval considered, the manuscript is in our opinion well-suited for the wide readership of *Marine Micropaleontology* and we therefore hope you will consider it for publication.

The manuscript contains original new results, data, ideas and interpretations not previously published nor under consideration for publication elsewhere (including electronic media and databases).

Yours sincerely,
Giuliana Villa

Possible reviewers:

- Shijun Jiang, Jinan University, Guangzhou, China - sjiang@jnu.edu.cn
- Carlotta Cappelli Dipartimento di Geoscienze via G. Gradenigo, 6 Universtià di Padova, Padova (Italy) -carlotta.cappelli@unipd.it
- Gary Wilson GNS New Zealand email: g.wilson@gmns.cri.nz
- Andrew Roberts, Australian National University, Research School of Earth Sciences College of Science andrew.roberts@anu.edu.au

Highlights

- Eocene-Oligocene sediments from ODP Hole 709C Indian ocean were investigated
- Nannofossil biostratigraphy and magnetostratigraphy of the area is established
- Two major hiatuses in the middle Eocene and across the EOT are identified
- Nannofossil assemblage record the Middle Eocene Climatic Optimum
- A shift from oligotrophic to eutrophic regime is recorded in the late Eocene

Abstract

We investigate the calcareous nannofossil biostratigraphy and magnetostratigraphy of middle Eocene – lower Oligocene sediments from ODP Hole 709 C.

The new bio-magnetostratigraphic analyses allow us to achieve accurate biochronology of the time interval spanning Chrons C20r (middle Eocene) to C12r, during which we identified 29 bioevents, in an about 12 Myr interval. The generally good magnetostratigraphic signal is less clear across the Eocene-Oligocene transition (EOT) but again reliable at the top of Chron C13n to Chron C12r (early Oligocene). Quantitative analyses on calcareous nannofossil assemblages allow recognizing the Middle Eocene Climatic Optimum (MECO) and the long cooling trend leading to the glacial state starting in the early Oligocene. We identify two hiatuses, in the lower middle Eocene and across the Eocene-Oligocene Transition (EOT).

Across the latter unconformity, a major transition from oligotrophic to eutrophic-favoring nannofossil taxa highlights an enhanced sea surface nutrient availability during the transition to the Oligocene glacial state. Finally, the late Oligocene warming event is evidenced at this site by an increase of warm-preferring calcareous nannofossil taxa.

Integrated calcareous nannofossil and magnetostratigraphic record of ODP Site 709: middle Eocene to late Oligocene paleoclimate and paleoceanography of the Equatorial Indian Ocean

Giuliana Villa [a*], Fabio Florindo [b,c], Davide Persico [a], Pontus Lurcock [b], Ana Paula de Martini[c], Luigi Jovane [c], and Chiara Fioroni. [d]

[*] Corresponding author

a) Università degli Studi di Parma, Dipartimento di Scienze Chimiche della Vita e della Sostenibilità ambientale, Parco Area delle Scienze, 157 a, 43124 Parma, Italy

b) Istituto Nazionale di Geofisica e Vulcanologia, Via di Vigna Murata 605, Roma 00143, Italy.

c) Instituto Oceanográfico, Universidade de São Paulo, Praça do Oceanográfico, 191, SP 05508-120, São Paulo, Brazil

d) Università degli Studi di Modena e Reggio Emilia, Dipartimento di Scienze Chimiche e Geologiche, Via Campi, 103, 41125 Modena, Italy.

Abstract

We investigate the calcareous nannofossil biostratigraphy and magnetostratigraphy of middle Eocene – lower Oligocene sediments from ODP Hole 709 C.

The new bio-magnetostratigraphic analyses allow us to achieve accurate biochronology of the time interval spanning Chrons C20r (middle Eocene) to C12r, during which we identified 29 bioevents, in an about 12 Myr interval. The generally good magnetostratigraphic signal is less clear across the Eocene-Oligocene transition (EOT) but again reliable at the top of Chron C13n to Chron C12r (early

Oligocene). Quantitative analyses on calcareous nannofossil assemblages allow recognizing the Middle Eocene Climatic Optimum (MECO) and the long cooling trend leading to the glacial state starting in the early Oligocene. We identify two hiatuses, in the lower middle Eocene and across the Eocene-Oligocene Transition (EOT).

Across the latter unconformity, a major transition from oligotrophic to eutrophic-favoring nannofossil taxa highlights an enhanced sea surface nutrient availability during the transition to the Oligocene glacial state. Finally, the late Oligocene warming event is evidenced at this site by an increase of warm-preferring calcareous nannofossil taxa.

Key words: Calcareous nannofossils, Eocene, Oligocene, Biomagnetostratigraphy, Paleoceanography, ODP Site 709

1. Introduction

Earth's climate underwent a distinct cooling trend from the early-middle Eocene to early Oligocene, with the emplacement of continental ice sheets on Antarctica (~34 Ma) (Francis et al., 2009; Liu et al., 2009; Bijl et al., 2013). This trend to cooler climates was punctuated by transient warming periods, of which the more prominent is the Middle Eocene Climatic Optimum (MECO; ~40 Ma) (Bohaty and Zachos, 2003; Jovane et al., 2007; Villa et al., 2008; Bohaty et al., 2009; Westerhold et al., 2020). The transition to glacial conditions, with the formation of a large and permanent East Antarctic Ice Sheet (EAIS), has been linked to a number of causes as

for instance the opening of Southern Ocean (SO) gateways (Kennett, 1977; Lagabrielle et al., 2009; Sarkar et al., 2019), which led to thermal isolation of Antarctica, the drawdown of pCO_2 (DeConto and Pollard, 2003; Pagani et al., 2005, 2011; Goldner et al., 2014; Kennedy-Asser et al., 2019), and/or a favorable orbital configuration which induced an insolation minimum (Coxall et al., 2005; Pälike et al., 2006).

The Eocene-Oligocene transition (EOT, described by Coxall and Pearson, 2007, and recently reviewed in detail by Hutchinson et al., 2020) encompasses the transition from a greenhouse to an icehouse world, and is characterized by a sudden and sizeable positive change in oxygen isotopic ($\delta^{18}O$) values of benthic foraminifera (Miller et al., 1987, Coxall and Wilson, 2011; Westerhold et al., 2020). This interval is also associated with a perturbation of the carbon cycle, an increase of primary productivity, a 1 km deepening of the Carbonate Compensation Depth (CCD) (Van Andel, 1975; Coxall and Pearson, 2007; Pälike et al., 2012), and a sea-level drop (Miller et al., 2008). Associated with the EOT a biotic turnover is also recorded, both in terrestrial (Hooker et al., 2004; Zanazzi et al., 2007) and in marine realms (Wade and Pearson, 2008; Dunkley Jones et al., 2008; Cotton and Pearson, 2011; Villa et al., 2014). These changes have been recorded in several oceanic sites at both high and low latitudes, but scarce data are available from the western Indian Ocean.

ODP Leg 115 was drilled in the Indian Ocean (Backman, Duncan et al., 1988) to achieve a south-north bathymetric transect and to investigate the Réunion volcanic system and the Paleogene to Quaternary stratigraphy. Site 709 is the shallowest in the

transect, well above the average CCD during the time interval considered in this work.

To this end, through high-resolution quantitative calcareous nannofossil and new magnetostratigraphic analyses, we compared the results with previous studies carried out in this region (Fioroni et al., 2015; Jones et al., 2019) and constructed a detailed middle Eocene-early Oligocene biochronology for the Equatorial Indian Ocean. In addition, calcareous nannofossils, as previously used to identify ocean latitudinal temperature gradients and productivity (Wei et al., 1992; Aubry, 1992, 1998; Bralower, 2002; Gibbs et al., 2006; Kalb and Bralower, 2012), enable us to reconstruct the paleoclimatic and paleoceanographic conditions through changes in the assemblages (e.g., Bralower, 2002; Persico and Villa, 2004; Villa et al., 2008; Villa et al., 2014) within a biomagnetostratigraphic framework.

2. Material and methods

Site 709 is located in the western equatorial Indian Ocean at 3°54.9'S and 60°33.1'E at a modern water depth of 3038.2 m on the Madingley Rise, a local topographic high between the Mascarene Plateau and the Carlsberg Ridge (Fig. 1) (Backman, Duncan, et al., 1988). Three holes were cored at this site, recovering a particularly homogeneous section of nannofossil ooze and chalk that ranges in age from the Eocene to the Holocene. The estimated paleodepth at Site 709 during the middle Eocene through the early Oligocene was constantly above the CCD (Touchard et al., 2003) with values approximately of 2200 m seafloor paleodepth in the middle Eocene (Bohaty et al.,

2009). Sediments generally have a high carbonate content ($CaCO_3$ wt%) ranging from about 85% to about 94%; a few samples have lower values. Hole 709C was cored to 353.7 meters below sea floor (mbsf), with a 93% recovery; this hole ended with nannofossil chalks of middle Eocene age (Backman, Duncan et al., 1988).

2.1 Calcareous Nannofossils

The micropaleontological analysis was performed on a set of 140 samples, from the working half of the split core Section 709C-29X-1, 28-29 (266.68 mbsf) to Section 709C-37X-7, 12-14,5 (353.13 mbsf). Sample resolution was approximately 20 cm in the interval from middle Eocene to early Oligocene, corresponding to a minimum temporal resolution of about 50kyr, but was lower in intervals with core disturbance. An upper Oligocene set of 17 samples (from Section 709C-28X-3 to Section 709C-22X-2) was taken at a lower resolution for paleoecological investigations.

Smear slides were prepared from unprocessed samples, following the standard technique (Bown and Young, 1998), and quantitative analyses were conducted in a polarized light microscope at 1250X magnification. For each sample at least 300 specimens were counted and classified (Villa et al., 2008) and two additional long traverses were scanned in order to identify rare taxa (Supplementary material A). The absolute abundance of each taxon was estimated by normalizing the number of the observed specimens to an area of 1 mm^2 (Villa et al., 2008), then plotted versus

depth. The number of specimens per mm^2 was used as an indicator of the total abundance of nannofossils in each sample.

The position of biozonal boundaries was calculated as the midpoint between two consecutive samples. The bioevents are indicated here as B (Base, lowest occurrence of the considered taxon), Bc (Base common, common and continuous presence of a taxon), T (top, highest occurrence of a taxon), Tc (top common) following Backman et al. (2012).

Nannofossils are usually well preserved but overgrowth is pronounced for some species (e.g.: *Discoaster* spp., *C. floridanus*), and other show a weak dissolution (e.g.: *Helicosphaera* spp.). Reworking is commonly present in some intervals of cores 115-709C-29, -32 (upper middle Eocene), and 115- 709C -33 (lower Oligocene), but it is negligible in the others.

The percentages of the different taxa were used to interpret the assemblage variation in terms of paleoecological changes, since their quantitative analysis is a key proxy for paleoceanographic reconstruction (Winter and Siesser, 1994; Gibbs et al., 2006; Kalb and Bralower, 2012; Villa et al., 2014). Dividing taxa with eutrophic affinity from those with warm/oligotrophic preference following Villa et al., 2014 and Fioroni et al., 2015 allowed to group the nannofossil species with the same paleoecological preference. These values were then plotted against depth to examine stratigraphic changes. Groups include only taxa with a well-known paleoecological preference, (Gibbs et al., 2006; Dunkley Jones et al., 2008; Villa et al., 2014, Fioroni et al., 2015; Jones et al., 2019, Cappelli et al., 2019) the warm-water taxa group

comprises *Discoaster* spp., *E. formosa*, and *Sphenolithus* spp.; the oligotrophic taxa group includes *Discoaster* spp., and *E. formosa;* the eutrophic taxa group consists of *R. daviesii*, *C. floridanus*, and *Reticulofenestra* spp. (i.e.: *R. dictyoda, R. samodurovi*, and *R. umbilicus*).

2.2 Paleomagnetism

Twenty-one advanced piston corer (APC) cores from Hole 709A, nine cores from Hole 709B and thirteen cores from Hole 709C were measured during the ODP cruise with the shipboard pass-through cryogenic magnetometer. The results were described as "erratic paleomagnetic data" and it was not possible to determine the reversal stratigraphy (Shipboard Scientific Party, 1988). Subsequently, Schneider and Kent (1990) investigated some intervals from Site 709; they reported that in general the results are of poor quality and determined a magnetostratigraphic record for two small portions along the retrieved succession: from ca. 15 to 35 mbsf (Pliocene-Pleistocene age) and from ca. 170 to 200 mbsf, near the Oligocene-Miocene boundary.

For this study, we collected one hundred and six oriented 7-cc plastic cubes at the Integrated Ocean Drilling Program (IODP) Kochi Core Center, Japan. All samples were taken from the working half of the split core sections 709C-31X-1 to -37X-7 (middle to late Eocene in age) between depths of 286.08 and 353.13 mbsf (meters below seafloor). We collected a second set of samples up to a depth of 266.7 mbsf to extend an analysis into the Oligocene portion of the hole. Both sets of samples were oriented only with respect to vertical, therefore absolute paleomagnetic declinations

could not be recovered for the polarity zonation.

Magnetic analyses were performed at the Istituto Nazionale di Geofisica e Vulcanologia (INGV) in Rome. Natural and artificial magnetizations were measured using a narrow-access pass-through 2-G Enterprises cryogenic magnetometer, with in-line alternating field (AF) demagnetization capability, housed in a magnetically shielded room. After measurement of the NRM, samples were demagnetized at successive peak AFs of 5, 10, 15, 20, 25, 30, 35, 40, 50, 60, 80 mT.

The stability of the natural remanent magnetization (NRM) was assessed using vector component diagrams (Zijderveld, 1967). Characteristic remanent magnetization (ChRM) directions were determined using principal component analysis (PCA) with linear best fits calculated from 3 or more demagnetization steps using the PuffinPlot paleomagnetic analysis application (Lurcock and Florindo, 2019).

Following AF demagnetization of the NRM, low-field magnetic susceptibility (κ) was measured using an AGICO KLY-2 Kappabridge magnetic susceptibility meter with a field of 0.1 mT at a frequency of 470 Hz. An anhysteretic remanent magnetization (ARM) was imparted by using a 0.05 mT direct current (DC) bias field superimposed on a 100mT peak AF and by translating samples through the AF and DC coil system at 10 cm/s, which is the lowest speed allowed by the control software.

Continuously monitored temperature dependence of the low-field magnetic susceptibility (κ) on a few milligrams of powdered samples (up to 700°C) was performed at the Instituto Oceanográfico da Universidade de São Paulo, Brazil. This was measured in air using a KLY-4 (AGICO) furnace-equipped Kappabridge, in order

to determine the characteristic Curie or Néel temperatures of magnetic minerals (Hrouda, 1994). The thermomagnetic curves were analysed using the Cureval8 program (http://www.agico.com).

2.3 Multivariate analyses on calcareous nannofossil assemblages

Using number of fossils/mm^2, dominance and species diversity (H Shannon-Weiner) were calculated by means of the software PAST (Hammer et al., 2001).

Multivariate R-mode Principal Component Analysis (PCA) was performed on the same quantitative database (nannofossils/mm^2) previously converted to natural logarithm, because percentage counts represent a closed set.

We identified the major components of the nannofossil assemblage using PCA. We graphically plotted the factors that explain the maximum variance, and we draw on paleoecologically interpretation from these relationships. The interpretation of the factors and their comparison with the abundance curves of the species allow to interpret the paleoecological behaviors of the nannofossil species in the stratigraphic sequence. This interpretation, combined with reference data from Villa et al. (2014), Fioroni et al. (2015), allowed us to subdivide the assemblage into paleoecological groups of species, as already described in section 2.1.

3. Results and discussion

3.1 Biohorizons

Previously published papers on nannofossil biostratigraphy of Site 709 were presented respectively by Okada (1990) for the Paleogene and Quaternary interval, and by Fornaciari et al. (1990) for the Oligo-Miocene interval. Here we provide a new highly resolved biostratigraphic framework based on calcareous nannofossils spanning from about 43.96 Ma (Top of *Pletolithus gigas,* Agnini et al., 2014, Cappelli et al., 2020) to 32.02 Ma (Top of *Reticulofenestra umbilicus*, Agnini et al., 2014) and thus covering a ca. 12 Myr interval.

Comparing our results with the nearby Site 711 (Fioroni et al., 2015) provides the opportunity to test the local reliability of the main biohorizons. However, the magnetostratigraphic data available at Site 711 has a low resolution because of the high number of samples (66% of the analysed samples) with no reliable magnetic directions (Savian et al., 2013). At Site 709, magnetostratigraphic results presented here are more detailed and accurate, and thus suitable to construct a reliable age model and determine correlations at global scale.

The main bioevents with their positions and the distribution patterns plotted against depth are summarized in Tab. 1 and in Fig. 2. A detailed discussion on each identified bioevent is available in the Appendix B.

3.2 Paleomagnetic behavior

NRM intensity ranges between 9.4×10^{-5} and 4.4×10^{-3} A/m with an average of 7.6×10^{-4} A/m. Two higher intensity intervals are located at 296.8 and at 308.7 mbsf

(Fig. 3). Downcore variations in NRM intensity and directions are not associated with variations of the concentration-dependent magnetic parameters κ and ARM (Fig. 3, 4). Stepwise AF demagnetization enabled isolation of the ChRM component for 95% of the samples analyzed, with maximum angular deviation (MAD) values between 0.81 and 10.6. Typical demagnetization behavior is shown in Figure 4. Most of the samples have a low-coercivity, normal polarity overprint that was successfully removed at peak fields of 10 mT. We interpret this overprint to have been acquired, as an isothermal remanent magnetization, during the drilling process and/or storage (e.g., Fuller et al., 1998). From observations made onboard, Schneider and Kent (1990) reported the presence of a remagnetization induced by the magnetized core barrels that mostly affected the external portions of the cores.

The ChRM inclinations enable delineation of magnetozones, which are defined, in most cases, using at least two consecutive samples with inclinations distinctly different from neighboring intervals (Fig. 5). In some magnetozones, occasional isolated samples have polarities opposite to those of the rest of the magnetozone (e.g., 298.28 mbsf, 322.48 mbsf). Such isolated samples were used with caution to define magnetozones and their correlation with the geomagnetic polarity time scale (GPTS) was inferred integrating biostratigraphic data.

The observed ChRM inclinations are steeper than the present-day geocentric axial dipole (GAD) inclination (±7.06°) at the site latitude and steeper than the expected GAD palaeoinclination (±4°) considering the calculated mean palaeolatitude (2.9°S, ±2.8°) of Hole 709C at 40 Ma (Torsvik et al., 2012; van Hinsbergen et al., 2015). A

similar inconsistency with the GAD predictions is present in the results obtained at the nearby ODP Site 711 by Savian et al. (2013). The authors interpreted this discrepancy due to some unresolved combination of unaccounted for motion of the plate, long-term non-dipole fields, and effects of hotspot motion on the plate circuit models. With the available data we cannot rule out that the discrepancy may be related to an unremoved overprint (e.g., Bowles, 2007).

Mean ChRM inclinations were computed separately for normal and reverse polarity populations using the Arason-Levi inclination-only algorithm (Arason and Levi, 2010) as implemented in the PuffinPlot application (Lurcock and Florindo, 2019). The normal polarity samples and the reverse polarity samples have a mean inclination of −36.3° (N = 39; α_{95} = 8.1°) and 41.8° (N = 64; α_{95}=5.4°), respectively**.** These values very narrowly fail an inclination-only reversals test at the 95% confidence level (since the antipode of the mean normal inclination lies 0.1° outside the 95% cone of confidence for the mean reversed direction), but the marginal nature of this result suggests that the mean directions could indeed represent a reliable polarity record.

3.2.1 Magnetic properties

Magnetic properties do not show substantial changes along the studied interval. The magnetic susceptibility ranges between -16 × 10^{-5} and 154 × 10^{-5} SI with a mean of 61.6 × 10^{-5} SI. The ARM, which is acquired by stable single domain magnetite, shows an average value of 6.8 × 10^{-3} A/m and ranges between 3.2 × 10^{-3} and 1.2 × 10^{-2} A/m

(Fig. 3). The relative stability of magnetic susceptibility and ARM suggests that this record does not have significant variations in magnetic mineral concentration.

Continuous monitoring of κ-*T* changes shows a change in slope (albeit noisy) at approximately 580°C. This suggests the ubiquitous presence of Fe spinels with a composition similar to magnetite (Fig. 3). The behavior of the discrete samples during AF demagnetization (Fig. 4) provides additional support for the presence of magnetite as the main magnetic carrier.

The observed increases in κ during heating are probably due to the thermally induced growth of new magnetite from iron-bearing clays (e.g., Hirt et al., 1993). The cooling curve has higher overall κ than the heating curve, which indicates production of new magnetic phases during heating.

3.3 Age Model and Magnetobiochronology

We provide an interpretation of the magnetic polarity pattern of Hole 709C from 266.7 to 353.13 mbsf, using the nannofossil bioevents observed throughout the section. Following the methodology proposed by Pälike et al. (2010) and afterwards applied by Agnini et al. (2014), the bioevents and the interpretation of the magnetic polarity pattern are calibrated against the orbitally tuned time scale of Pälike et al. (2006) from the base of Chron C12r (33.157 Ma) to the base of Chron C19n (41.510 Ma), and with the GPTS of Cande and Kent (1995) between the top of Chron C20n

(42.536 Ma) and the base of Chron C20r (46.264 Ma). The age-depth plot and the magnetobiostratigraphic framework are presented in Figures 6 and 7, respectively.

The combined bio- and magnetostratigraphy results highlight at least two relevant hiatuses. The first hiatus is located between Chron C19r and Chron C18r and the single normal polarity sample at 322.48 mbsf could represent a portion of Chron C19n. The presence of the lower part of Chron C19r at 328.37 mbsf is confirmed by the Bc of *Cribrocentrum reticulatum* at 323.13 mbsf (Agnini et al., 2014). The hiatus of at least 1 Myr, from the Bc of *C. reticulatum* and the top of Chron C19n. A second hiatus, at ca. 285 mbsf, is highlighted by the concurrent extinctions of *Discoaster barbadiensis*, *D. saipanensis,* whose Tops are at 34.77 Ma and at 34.44 Ma respectively, *C. reticulatum* (Top at 35.24 Ma, according to Agnini et al. 2014), and *Cribrocentrum isabellae* (Fornaciari et al., 2010) (Figs. 2, 6). Based on calcareous nannofossil data, this hiatus spans at least Zone CNE20 biozone. In contrast, at the nearby Site 711, the nominate bioevents (i.e., *Discoaste*r spp., *C. reticulatum*, and *Clausicoccus* spp.) occur stratigraphically close each other, but clearly spaced (Fioroni et al., 2015). At Site 711, the availability of a good magnetostratigraphic record during this time interval confirms these data (Savian et al., 2013); in particular, the Top of *C. reticulatum* is detected in Chron C15n, whereas the top of the "rosette shaped" *Discoaster* group is recorded in Chron C13r. The continuous and relatively more expanded record at Site 711 is possibly explained by less effective role played by the bottom paleocurrents at deeper depths rather than at shallower depositional setting (Site 709).

In addition, at Site 709 just above the hiatus, we detect a noticeable increase in *Clausicoccus* spp. (Fig. 2). Due to overgrowth due to the high carbonate content, specimens of this genus were not recognized at species level, however, based on the mean size of the specimens, we are confident that the increase is mainly composed of *C. subdistichus*. The acme beginning of this species is reported with an age of 33.88 Ma, indicating the base of Zone CNO1 (Agnini et al., 2014) and suggesting that the unconformity also includes Zone CNE21.

3.4 Multivariate analysis

To determine the dominance and Shannon-Wiener diversity index (H) the nannofossil abundance is tested to evaluate the response to environmental forcing.

The interpretation of the PCA factors is based on graphic comparison with the considered paleoecological indicative taxa (Fig. 8) and by estimating the SST and the nutrient concentration (Fig. 9). The indices show fairly stable values from the base up to about 292 mbsf. At this depth, the dominance index and H Shannon diversity index show, respectively, increasing and decreasing trends, revealing a change typical of an environmental condition variation. The general trend towards a decline in specific diversity suggests a cooling trend from the middle Eocene to the early Oligocene (Bown et al., 2008; Cronin and Cronin, 2015).

The PCA analyses of the census data show that two significant principal components (PCA1 and PCA2) explain 77% of the variance (Fig. 9). The PC1 scores (PC1, 61.77%

of the variance) display a clear shift from negative to positive values at 320 mbsf, at the base of C18r (41.358 Ma) (Fig. 9). This trend is interrupted only at 315 mbsf by a short negative peak, dated at about 40 Ma. The overall PC1 trend is reminiscent of the $\delta^{18}O$ records from several sites indicative of the paleoclimate evolution of the middle Eocene (Bohaty et al., 2009). Therefore, we associate PC1 with the paleoclimatic factor SST. The positive shift at 320 mbsf should therefore correspond to the pre-MECO cooling event (Bohaty et al., 2009; Savian et al., 2016). We interpret the negative peak at 315 mbsf, likely to coincide with the MECO, while upward, cooling conditions prevail.

The PCA factor 2 (PC2, 15.39% of the variance) is dominated by positive scores up to 287 mbsf where it records an abrupt variation to negative values. Based on the correlation with nannofossil associations, we interpret this index to indicate trophic conditions of the surface waters (see § 3.5.3).

3.5 Nannofossil relative abundance as response to middle Eocene - late Oligocene climate variability

The paleoecological interpretation is based on the relative abundance of the key taxa and on groups of taxa with the same preference treated with a statistical approach (Figs. 8, 9).

3.5.1 The Middle Eocene Climatic Optimum

A peak in warm/oligotrophic-water taxa is identified at approximately 315 mbsf, corresponding to an age of about 40 Ma (Fig. 9). This timing is consistent with the MECO event (Jovane et al., 2007; Villa et al., 2008; Bohaty et al., 2009; Boscolo Galazzo et al., 2014). This peak is the highest value in warm/oligotrophic taxa, before the beginning of the late Eocene trend in which these taxa decrease prior to the EOT. The available $\delta^{18}O$ stable isotope data (Baker et al., 1990) have an extremely low resolution for the identification of this transient warming event, and future work should focus on obtaining a light stable isotope chemostratigraphy. PCA factor 1 (variance 61%) fits well with the warm taxa curve, and we interpret that it records SST variation (Fig. 9).

3.5.2 The "Cooling C" Event (or Priabonian oxygen maximum)

At ~ 295 mbsf we notice a decrease in warm-water taxa (Fig. 9). This level correlates with Subchron C17n.1n and an age of ~37 Ma. This change has been correlated to the Priabonian oxygen isotope maximum (PrOM, Scher et al., 2014, Pascher et al., 2015) which has been interpreted as a cooling event which might have resulted in a possible onset of widespread glaciation of Antarctica (Carter et al., 2017). In terms of nannofossil assemblages, this paleoclimatic change has been detected for the first time in the Southern Ocean (Villa et al., 2008, 2014) and referred to as "Cooling C" Event. Just above the warm-water taxa decrease, an increase in dominance and

simultaneous decrease in diversity was observed (Fig. 9) and associated with an early expansion of the Antarctic ice sheet recorded at low latitudes.

3.5.3 The late Eocene to early Oligocene

Although the very low sedimentation rate makes data difficult to interpret, the decrease in warm/oligotrophic taxa is noteworthy. The change in the PCA Factor 2 toward negative values, from ~ 287 mbsf (about 35.2 Ma), at the base of Chron C15n is also noteworthy. As discussed in § 3.4, these modifications indicate a change in the surface nutrient regime, from oligotrophic to more eutrophic surface waters (Fig. 9). This result is related to the initiation of a proto-Antarctic Circumpolar Current (ACC) at ~ 35.5 Ma (Sarkar et al., 2019), as well as invigorated surface and bottom paleocurrents around Antarctica starting from about 35.7 Ma (Houben et al., 2019, Barker et al., 2007).

At 285 mbsf a relevant change in the nannofossil assemblage is identified in correspondence of the hiatus juxtaposing common upper Eocene oligotrophic-taxa with common lower Oligocene eutrophic-taxa and indicating a reorganization of the sea surface nutrient regime. The hiatus includes at least the entire Chron C13r, and prevents to identify the exact extent and position of the assemblage change. In fact, the hiatus has likely completely erased the profound reorganization in the nannofossil assemblage recorded at Site 711 (Fioroni et al., 2015) in the late Eocene Chron C13r, that has been also detected in Tanzania (Dunkley Jones et al., 2008), Java (Jones et

al., 2019), and in the tropical Atlantic (Ravizza and Paquay, 2008). This assemblage variation indicates a measurable response of nannofossils to increased sea surface nutrient availability in the equatorial Indian Ocean and is possibly linked to the formation at high latitudes of nutrient-rich waters. In particular, the Subantarctic Mode Water (SAMW) is a water mass formed in the Southern Ocean by deep mixing, which sinks below the ocean surface and moves northward, carrying a large amount of regenerated nutrients to lower latitudes (Sarmiento et al., 2004). Changes in ocean paleocirculation, precursors of the major glaciation at Oi-1, triggered enhanced mixing also at low latitudes, and consequently produced enhanced eutrophication of sea surface waters evidenced by nannofossil turnover, well before the EOT.

3.5.4 The late Oligocene warming

The lower resolution data set collected from ~ 270 to ~ 200 mbsf was analysed to detect variations during the Oligocene. Warm and oligotrophic taxa, after the decrease at the EOT, show a gradual increase through the Oligocene, peaking at about 210 mbsf (Fig. 10). We infer this increase corresponds to the Late Oligocene warming event, previously detected in the Southern Ocean using nannofossil assemblage variation (Villa and Persico, 2006) and by oxygen isotopes (Pekar et al., 2006), and recently also recognized in the Tibetan Plateau through pollen assemblage variations (Wu et al., 2018), suggesting a global response to this event.

4. Conclusions

The integrated calcareous nannofossil and magnetostratigraphic records allow constructing a robust chronostratigraphic framework. Despite the presence of two hiatuses in the middle Eocene and across the EOT, the ODP Site 709 record provides evidence of important changes in climate and oceanography at low latitudes during this critical time interval. Nannofossil assemblages record the MECO event (*sensu* Bohaty et al., 2009) at this Site including both the pre-MECO cooling and the warm peak at about 40 Ma.

A transient decline in warm water taxa at about 37 Ma has been correlated to the "Cooling Event C" that paves the way for the major climatic deterioration occurred during the EOT.

Prominent changes in Southern Ocean circulation related to the geographic isolation of Antarctica and invigorated bottom water currents in the late Eocene led to increased upwelling and enhanced nutrient supply at low latitudes. This change in nutrient supply is recorded in the shift from prevailing late Eocene oligotrophic to early Oligocene eutrophic assemblages.

An increase in warm water nannofossil taxa in the late Oligocene suggests a warming event at equatorial latitudes prior to the cooling at the Oligocene/Miocene boundary.

Acknowledgements

We thank the Integrated Ocean Drilling Program (IODP) for providing access to the studied cores. The IODP is sponsored by the U.S. National Science Foundation (NSF) and participating countries under the management of Joint Oceanographic Institutions, Inc.

This work has benefited from the equipment and framework of the COMP-HUB Initiative, funded by the 'Departments of Excellence' programme of the Italian Ministry for Education, University and Research (MIUR, 2018-2022)

L.J. has been supported by Fundação de Amparo a Pesquisa do Estado de São Paulo (FAPESP) grant 2016/24946-9 and by the Coordenação de Aperfeiçoamento de Pessoal de Nível Superior - Brasil (CAPES) - Finance Code 001.

References

Agnini, C., Fornaciari, E., Raffi, I., Catanzariti, R., Pälike, H., Backman, J., Rio, D., 2014. Biozonation and biochronology of Paleogene calcareous nannofossils from low and middle latitudes. Newsletters on Stratigraphy, 47, 131–181. https://doi.org/10.1127/0078- 0421/ 2014/0042.

Arason, Þ., Levi, S., 2010. Maximum likelihood solution for inclination-only data in paleomagnetism. Geophysical Journal International, 182(2), 753–771. https://doi.org/10.1111/j.1365-246X.2010.04671.x.

Aubry, M.P., 1992. Late Paleogene nannoplankton evolution: A tale of climatic deterioration, in Eocene-Oligocene Climatic and Biotic Evolution, edited by D. R. Prothero and W. A. Berggren, Princeton Univ. Press, Princeton, 272–309.

Aubry, M.P., 1998. Early Paleogene calcareous nannoplankton evolution: a tale of climatic amelioration. In: Aubry, M.-P., Lucas, S. G., Berggren, W. A. (Eds.), Late Paleocene–early Eocene Biotic and Climatic Events in the Marine and Terrestrial Records. Columbia University Press, New York, 158–201.

Backman, J., Duncan, R.A., et al., 1988. Proc. ODP, Init. Repts., 115: College Station, TX (Ocean Drilling Program). p 459–588. doi:10.2973/odp.proc.ir.115.108.1988.

Backman, J., Raffi, I., Rio, D., Fornaciari, E., Palike, H., 2012. Biozonation and biochronology of Miocene through Pleistocene calcareous nannofossils from low and middle latitudes. Newsletters on Stratigraphy 45, 221–244. doi:10.1127/0078-0421/2012/0022.

Baker, P.A., Malone, M.J., Burns, S.J., Swart, P.K., 1990. Minor element and stable isotopic composition of the carbonate fine fraction: Site 709, Indian Ocean. In: Duncan, R. A., Backman, J., Peterson, L. C., et al., 1990. *Proc. ODP, Sci. Results,* 115: College Station, TX (Ocean Drilling Program). 661-675.

Barker, P.F., Filippelli, G.M., Florindo, F., Martin, E., Scher, H.D., 2007. Onset and role of the Antarctic Circumpolar Current, Deep Sea Res., Part II, 54, 2388–2398.

Bijl, P.K., Bendle, J.A., Bohaty, S.M., Pross, J., Schouten, S., Tauxe, L., Stickley, C.E., McKay, R.M., Röhl, U., and Olney, M. 2013. Eocene cooling linked to early flow across the Tasmanian Gateway, P. Natl. Acad. Sci. USA, 110, 9645–9650.

Bohaty, S.M., and Zachos, J.C., 2003, Significant Southern Ocean warming event in the late middle Eocene: Geology, v. 31, 1017–1020, doi: 10.1130/G19800.1.

Bohaty, S.M., Zachos, J.C., Florindo, F., Delaney, M.L., 2009. Coupled greenhouse warming and deep-sea acidification in the middle Eocene, Paleoceanography, 24, PA2207. 16 doi:10.1029/2008PA001676.

Boscolo Galazzo, F., Thomas, E., Pagani, M., Warren, C., Luciani, V., Giusberti, L., 2014. The middle Eocene climatic optimum (MECO): A multiproxy record of paleoceanographic changes in the southeast Atlantic (ODP Site 1263, Walvis Ridge), Paleoceanography, 29. 1143–1161. doi:10.1002/2014PA002670.

Bowles, J., 2007. Coring-related deformation of Leg 208 sediments from Walvis Ridge: Implications for paleomagnetic data, Physics of the Earth and Planetary Interiors, 161, 161-169.

Bown, P.R., Dunkley Jones, T., Lees, J.A., Pearson, P.N., Randell, R., Coxall, H.K., Mizzi, J., Nicholas, C., Karega, A., Singano, J., Wade, B.S., 2008. A calcareous microfossil Konservat Lagerstatte from the Paleogene Kilwa Group of coastal Tanzania. GSA Bulletin 120. 3–12.

Bown, P.R., Young, J.R., 1998. Techniques. In: Bown, P.R., Ed., Calcareous Nannofossil Biostratigraphy (British Micropalaeontological Society Publications Series), Chapman and Kluwer Academic, London, 16-28.

Bralower, T.J., 2002. Evidence of surface water oligotrophy during the Paleocene–Eocene thermal maximum: Nannofossil assemblage data from Ocean Drilling Program Site 690, Maud Rise, Weddell Sea, Paleoceanography, 17(2). 1023 doi:10.1029/2001PA000662.

Cande, S.C., Kent, D.V., 1995. Revised calibration of the geomagnetic polarity timescale for the Late Cretaceous and Cenozoic. Journal of Geophysical Research 100. 6093 - 6095.

Cappelli, C., Bown, P., R., Westerhold, T., Bohaty, S., M., De Riu, M., Lobba, V., Yamamoto, Y., Agnini, C., 2019. The early to middle Eocene transition: an integrated calcareous nannofossil and stable isotope record from the Northwest Atlantic Ocean (IODP Site U1410). Paleoceanography and Paleoclimatology, 34 (12), 1913-1930 doi:10.1029/2019PA003686.

Carter, A., Riley, T.R., Hillenbrand C.-D., Rittner, M., 2017. Widespread Antarctic glaciation during the Late Eocene. Earth and Planet. Sci. Letters, 458, 49-57. http://dx.doi.org/10.1016/j.epsl.2016.10.045

Cotton, L. J., Pearson, P., 2011. Extinction of larger foraminifera at the Eocene/Oligocene boundary. Palaeogeogr. Palaeoclimatol. Palaeoecol. 281-296 doi:10.1016/j.palaeo.2011.09.008.

Coxall, H.K., Wilson, P.A., Pälike, H., Lear, C.H., Backman, J., 2005. Rapid stepwise onset of Antarctic glaciation and deeper calcite compensation in the Pacific Ocean. Nature, 433(7021). 53–57. https://doi.org/10.1038/nature03135.

Coxall, H.K., Pearson, P.N., 2007. The Eocene-Oligocene transition. In: Williams, M. et al. eds. Deep-Time Perspectives on Climate Change: Marrying the Signal from Computer Models and Biological Proxies. Micropaleontology Society Special Publication London: Geological Society. 351-387.

Coxall, H. K. & Wilson, P. A. 2011. Early Oligocene glaciation and productivity in the eastern equatorial Pacific: insights into global carbon cycling. Paleoceanography, 26, PA2221.

Cronin, T.M., Cronin, M.A., 2015. Biological response to climate change in the Arctic Ocean: the view from the past. Arktos 1, 4. doi:10.1007/s41063-015-0019-3.

DeConto, R.M., Pollard D., 2003. Rapid Cenozoic glaciation of Antarctica induced by declining atmospheric CO2, Nature, 421. 245–249.

Dunkley Jones, T., Bown, P.R., Pearson, P.N., Wade, B.S., Coxall, H.K., Lear, C.H., 2008. Major shifts in calcareous phytoplankton assemblages through the Eocene-Oligocene transition of Tanzania and their implications for low- latitude primary production. Paleoceanography, 23, PA4204. 14 https://doi.org/10.1029/2008PA001640.

Fioroni, C., Villa, G., Persico, D., Jovane, L., 2015. Middle Eocene- Lower Oligocene calcareous nannofossil biostratigraphy and paleoceanographic implications from Site 711 (equatorial Indian Ocean). Marine Micropaleontology, 118. 50–62. https://doi.org/10.1016/j. marmicro.2015.06.001.

Fornaciari, E., Raffi, I., Rio, D., Villa, G., Backman, J., Olafsson, G., 1990. Quantitative distribution patterns of Oligocene and Miocene calcareous nannofossils from the western equatorial Indian Ocean. In: Duncan, R. A., Backman, J., Peterson, L. C., et al., Proceedings ODP, Scientific Results 115 (Ocean Drilling Program, College Station, TX). 237–254. doi:10.2973/odp.proc.sr.115.153.

Fornaciari, E., Agnini, C., Catanzariti, R., Rio, D., Bolla, E. M., Valvasoni, E., 2010. Mid- latitude calcareous nannofossil biostratigraphy and biochronology across the middle to late Eocene transition. Stratigraphy, 7(4). 229–264. https://doi.org/10.1128/AAC.8.6.617.

Francis, J.E., Marenssi, S., Levy, R., Hambrey, M., Thorn, V.C., Mohr, B., Brinkhuis, H., Warnaar, J., Zachos, J., Bohaty, S. and DeConto, R., 2009. From Greenhouse to

Icehouse – The Eocene/Oligocene in Antarctica. In: Fabio Florindo and Martin Siegert, editors: Developments in Earth and Environmental Sciences, Vol 8, Antarctic Climate Evolution, Fabio Florindo and Martin Siegert. The Netherlands: Elsevier, 2009. 309–368. doi: 10.1016/S1571-9197(08)00008-6.

Fuller, M., Hastedt, M., Herr B., 1998. Coring-induced magnetization of recovered sediment. In: Weaver, P.P.E., Schmincke, H.-U., Firth, J.V., Duffield, W. (Eds.), Proc. ODP, Sci. Res., Vol. 157. Ocean Drilling Program, College Station, TX, 47-56.

Gibbs, S.J., Bralower, T.J., Bown, P.R., Zachos, J.C., Bybell, L.M., 2006. Shelf and open ocean calcareous phytoplankton assemblages across the Paleocene-Eocene thermal maximum: implications for global productivity gradients. Geology 34. 233–236. http://dx.doi.org/10.1130/G22381.1.

Goldner, A., Herold, N., Huber, M., 2014. Antarctic glaciation caused ocean circulation changes at the Eocene- Oligocene transition. Nature, 511(7511), 574–577. https://doi.org/10.1038/nature13597.

Hammer, Ø., Harper, D.A.T., Ryan P.D., 2001. PAST: Paleontological statistics software package for education and data analysis, Palaeontol. Electron., 4, 9. 1-9.

Hirt, A.M., Banin, A., and Gehring, A.U., 1993. Thermal generation of ferromagnetic minerals from iron-enriched smectites. Geophys. J. Int. 115, 1161-1168.

Hooker, J.J., Collinson, M.E., Sille, N.P., 2004. Eocene-Oligocene mammalian faunal turnover in the Hampshire Basin, UK: Calibration to the global time scale and the major cooling event. Journal of the Geological Society 161(2). 161-172. DOI:10.1144/0016-764903-091.

Houben, A.J.P., Bijl, P.K., Sluijs, A., Schouten, S., Brinkhuis, H., 2019. Late Eocene Southern Ocean cooling and invigoration of circulation preconditioned Antarctica for full- scale glaciation. Geochemistry, Geophysics, Geosystems, 20, 2214–2234. https://doi. org/10.1029/2019GC008182.

Hrouda, F., 1994. A technique for the measurement of thermal changes of magnetic susceptibility of weakly magnetic rocks by the CS-2 apparatus and KLY-2 Kappabridge, Geophys. J. Int., 118, 604–612.

Hutchinson, D. K., Coxall, H. K., Lunt, D. J., Steinthorsdottir, M., de Boer, A. M., Baatsen, M., von der Heydt, A., Huber, M., Kennedy-Asser, A. T., Kunzmann, L., Ladant, J.-B., Lear, C. H., Moraweck, K., Pearson, P. N., Piga, E., Pound, M. J., Salzmann, U., Scher, H. D., Sijp, W. P., Śliwińska, K. K., Wilson, P. A., Zhang, Z. The Eocene-Oligocene transition: a review of marine and terrestrial proxy data, models and model-data comparisons, Clim. Past Discuss., https://doi.org/10.5194/cp-

2020-68, in review, 2020.

Jones, A.P., Dunkley Jones, T., Coxall, H., Pearson, P.N., Nala, D., Hoggett, M., 2019. Low- latitude calcareous nannofossil response in the Indo- Pacific Warm Pool across the Eocene- Oligocene Transition of Java, Indonesia. Paleoceanography and Paleoclimatology, 34, 1833–1847. https://doi.org/10.1029/2019PA003597.

Jovane, L., Florindo, F., Coccioni, R., Dinares-Turell, J., Marsili, A., Monechi, S., Roberts, A.P., Sprovieri, M., 2007. The middle Eocene climatic optimum event in the Contessa Highway section, Umbrian Apennines, Italy. Geol. Soc. Am. Bull. 119 (3). 413–427. http://dx.doi.org/10.1130/B25917.1.

Kalb, A.L., Bralower, T.J., 2012. Nannoplankton origination events and environmental changes in the late Paleocene and early Eocene. Marine Micropaleontol. v. 92. 1–15. http://dx.doi.org/10.1016/j.marmicro.2012.03.003.

Kennedy- Asser, A.T., Lunt, D.J., Farnsworth, A., Valdes, P.J., 2019. Assessing mechanisms and uncertainty in modelled climatic change at the Eocene- Oligocene transition. Paleoceanography and Paleoclimatology, 34. 16–34. https://doi. org/10.1029/2018PA003380.

Kennett, J. P., 1977. Cenozoic evolution of Antarctic glaciation, circum-Antarctic ocean, and their impact on global paleoceanography. J. Geophys. Res., 82. 3843–3860.

Lagabrielle, Y., Goddéris, Y., Donnadieu, Y., Malavieille, J., Suarez, M., 2009. The tectonic history of Drake Passage and its possible impacts on global climate, Earth Planet. Sci. Lett., 279. 197–211. doi:10.1016/j.epsl.2008.12.037.

Liu, Z., Pagani, M., Zinniker, D., Deconto, R.M., Huber, M., Brinkhuis, H., et al., 2009. Eocene- Oligocene climate transition. Science (New York, N.Y.), 323(February). 1187–1190. https://doi.org/10.1126/science.1166368.

Lurcock, P. C., Florindo, F., 2019. New developments in the Puffin Plot paleomagnetic data analysis program. Geochemistry, Geophysics, Geosystems, 20. 5578-5587. https://doi.org/10.1029/2019GC008537.

Miller, K.G., Fairbanks, R.G., Mountain, G.S., 1987. Tertiary oxygen isotope synthesis,
sea-level history and continental margin erosion. Paleoceanography 2. 1–19.

Miller, K.G., Browning, J.V., Aubry, M.P., Wade, B.S., Katz, M.E., Kulpecz, A.A., Wright, J.D., 2008. Eocene-Oligocene global climate and sea-level change: St. Stephens Quarry, Alabama. GSA Bulletin, 120, 34-53. doi: 10.1130/B26105.1.

Okada, H., 1990. Quaternary and Paleogene calcareous nannofossils, Leg 115. In: Duncan, R.A., Backman, J., Peterson, L.C., et al. (Eds.), Proceedings ODP. Scientific Results 115. Ocean Drilling Program, College Station, TX, 129–174.

Pagani, M., Zachos J.C., Freeman K.H., Tipple B., Bohaty, S.M., 2005. Marked decline in atmospheric carbon dioxide concentrations during the Paleogene. Science, 309. 600–603, doi:10.1126/science.1110063.

Pagani, M., Huber, M., Liu, Z., Bohaty, S.M., Henderiks, J., Sijp, W., et al., 2011. The role of carbon dioxide during the onset of antarctic glaciation. Science, 334(6060). 1261–1264. https://doi.org/10.1126/science.1203909.

Pälike, H., Norris, R.D., Herrle, J.O., Wilson, P.A., Coxall, H.K., Lear, C.H., Shackleton, N.J., Tripati, A.K., Wade, B.S., 2006. The heartbeat of the Oligocene climate system, Science, 314. 1894–1898, doi:10.1126/science.1133822.

Pälike, H., Lyle, M., Nishi, H., Raffi, I., Gamage, K., Klaus, A., and the Expedition 320/321 Scientists, 2010. Proc. IODP, 320/321: Tokyo (Integrated Ocean Drilling Program Management International, Inc.). doi:10.2204/iodp.proc.320321.2010

Pälike, H., Lyle, M.W., Nishi, H., Raffi, I., Ridgwell, A., Gamage, K., Baldauf, J., et al., 2012. A Cenozoic record of the equatorial Pacific carbonate compensation depth, Nature, 488, 609–614, doi:10.1038/nature11360.

Pascher K.M., Hollis, C.J., Bohaty, S.M., Cortese, G., McKay, R.M., Seebeck, H., Suzuki, N., Chiba, K., 2015. Expansion and diversification of high-latitude radiolarian assemblages in the late Eocene linked to a cooling event in the southwest Pacific. Clim. Past, 11. 1599–1620. www.climpast.net/11/1599/2015/. doi:10.5194/cp-11-1599-2015.

Pekar, S.F., DeConto, R., Harwood, D.M., 2006, Resolving a late Oligocene conundrum: Deep-sea warming versus Antarctic glaciation. Palaeogeogr. Palaeoclimatol. Palaeoecol., 231. 29–40. doi:10.1016/j.palaeo.2005.07.024.

Persico, D., Villa, G., 2004. Eocene–Oligocene calcareous nannofossils from Maud Rise and Kerguelen Plateau /Antarctica: Paleoecological and paleoceanographic implications, Marine Micropaleontol. v. 52. 153–179. doi:10.1016/j.marmicro.2004.05.002..

Ravizza, G., Paquay, F., 2008. Os isotope chemostratigraphy applied to organic rich marine sediments from the Eocene-Oligocene transition on the West African margin (ODP Site 959). Paleoceanography, 23, PA2204. doi:10.1029/2007PA001460.

Sarkar, S., Basak, C., Frank, M., Berndt, C., Huuse, M., Badhani, S., Bialas, J., 2019. Late Eocene onset of the Proto- Antarctic Circumpolar Current. Nature Sci. Rep.9, 10125, https://doi.org/10.1038/s41598-019-46253-1.

Sarmiento, J.L., Gruber, N., Brzezinski, M.A., Dunne, J.P., 2004. High-latitude controls of thermocline nutrients and low latitude biological productivity. Nature 427. 56–60.

Savian, J.F., Jovane, L., Bohaty, S.M., Wilson, P.A., 2013. Middle Eocene to early Oligocene magnetostratigraphy of ODP Hole 711A (Leg 115), western equatorial Indian Ocean. Geol. Soc. Lond. Spec. Publ. 373. p.97-110. http://dx.doi.org/10.1144/SP373.16.

Savian, J.F., Jovane, L., Giorgioni, M., Iacoviello, F., Rodelli, D., Roberts, A.P., Chang, L., Florindo, F., Sprovieri M., 2016. Environmental magnetic implications of magnetofossil occurrence during the Middle Eocene Climatic Optimum (MECO) in pelagic sediments from the equatorial Indian Ocean. Palaeogeography, palaeoclimatology, palaeoecology. 441, 212-222. https://doi.org/10.1016/j.palaeo.2015.06.029

Scher, H.D., Bohaty, S.M., Smith, B.W., Munn, G. H., 2014. Isotopic interrogation of a suspected late Eocene glaciation. Paleoceanography, 29, 628–644. https://doi.org/10.1002/2014PA002648.

Schneider, D.A., Kent, D.V., 1990. Paleomagnetism of Leg 115 sediments: implications for Neogene magnetostratigraphy and paleolatitude of the Réunion Hotspot. In: Duncan, RA; Backmann, J; Peterson, LC; et al. (eds.), Proceedings of the Ocean Drilling Program, Scientific Results, College Station, TX (Ocean Drilling Program), v. 115. 717-736, https://doi.org/10.2973/odp.proc.sr.115.197.1990.

Shipboard Scientific Party, 1988. Site 709. *In* Backman, J., Duncan, R.A., et al., *Proc. ODP*, *Init. Repts.*, 115: College Station, TX (Ocean Drilling Program), 459–588. doi:10.2973/odp.proc.ir.115.108.1988

Touchard, Y., Rochette, P., Aubry, M.P., Michard, A., 2003. High-resolution magnetostratigraphic and biostratigraphic study of Ethiopian traps-related products in Oligocene sediments from the Indian Ocean. Earth Planet. Sci. Lett., 206. 493-508.

Torsvik, T.H, Van der Voo, R., Preeden, U., MacNiocaill, C., Steinberger, B., Doubrovine, P., et al., 2012. Phanerozoic polar wander, palaeogeography and dynamics. Earth-Science Reviews 114. 325-368.

Van Andel, T.H., 1975, Mesozoic/Cenozoic calcite compensation depth and the global distribution of calcareous sediments, Earth Planet. Sci. Lett., 26. 187–194.

van Hinsbergen, D.J., de Groot, L.V., van Schaik, S.J., Spakman, W., Bijl, P.K., Sluijs, A., Langereis, C.G., Brinkhuis, H., 2015. A Paleolatitude Calculator for Paleoclimate Studies (model version 2.1), PLOS ONE. 21 p.

Villa, G., Persico, D., 2006. Late Oligocene climatic changes: Evidence from calcareous nannofossils at Kerguelen Plateau Site 748 (Southern Ocean), Palaeogeogr. Palaeoclimatol. Palaeoecol., 231. 110–119. doi:10.1016/j.palaeo.2005.07.028.

Villa, G., Fioroni, C., Pea, L., Bohaty, S.M., Persico, D., 2008. Middle Eocene–late Oligocene climate variability: Calcareous nannofossil response at Kerguelen Plateau, Site 748, Marine Micropaleontol., 69. 173–192. doi:10.1016/j.marmicro.2008.07.006.

Villa, G., Fioroni, C., Persico, D., Roberts, A.R., Florindo, F., 2014. Middle Eocene to Late Oligocene Antarctic glaciation/deglaciation and Southern Ocean productivity. Paleoceanography 29. 223–237. http://dx.doi.org/10.1002/2013PA002518.

Wade, B., Pearson, P., 2008. Planktonic foraminiferal turnover, diversity fluctuations and geochemical signals across the Eocene/Oligocene boundary in Tanzania. Marine Micropaleontology, 68. 244-255. doi:10.1016/j.marmicro.2008.04.002.

Wei, W., Villa, G., Wise Jr., S.W., 1992. Paleoceanographic implications of Eocene-Oligocene calcareous nannofossils from Sites 711 and 748 in the Indian Ocean. In: Wise Jr., S.W., Schlich, R., et al. (Eds.), Proc. ODP. Scientific Results 120. 979–999.

Westerhold, T., Marwan, N., Drury, A.J., Liebrand, D., Agnini, C., Anagnostou, E., Barnet, J.S.K., Bohaty, S.M., De Vleeschouwer, D., Florindo, F., Frederichs, T., Hodell, D.A., Holbourn, A.E., Kroon, D., Lauretano, V., Littler, K., Lourens, L.J., Lyle, M., Pälike, H., Röhl, U., Tian, J., Wilkens, R.H., Wilson, P.A., Zachos, J.C. 2020. An astronomically dated record of Earth's climate and its predictability over the last 66 million years. Science. doi: 10.1126/science.aba6853

Winter, A., Siesser, W.G., 1994. Coccolithophores. Cambridge Univ. Press, Cambridge. 242 p.

Wu, F., Miao, Y., Meng, Q., Fang, X., Sun, J., 2018. Late Oligocene Tibetan Plateau warming and humidity: Evidence from a sporopollen record. Geochemistry, Geophysics, Geosystems, 20. 434–441. https://doi.org/10.1029/ 2018GC007775.

Zanazzi, A., Kohn, M.J., MacFadden, B.J., Terry, D.O., 2007. Large temperature drop across the Eocene-Oligocene transition in central North America. Nature 445. 639–642.

Zijderveld, J. D. A. (1967), A. C. demagnetization of rocks: Analysis of results, in Methods in Palaeomagnetism, Dev. in Solid Earth Geophys., edited by D. W. Collinson, K. M. Creer, and S. K. Runcorn, 254–286, Elsevier, Amsterdam.

FIGURE CAPTIONS:

Fig. 1: Location of the studied site (ODP Site 709) and of the nearby ODP Site 711.

Fig. 2: Abundance patterns of calcareous nannofossil index species at ODP Site 709 plotted against depth (mbsf) and expressed as number of specimens/mm^2

Fig. 3: Stratigraphic variations of intensity of (a) NRM and NRM@10mT, (b) k, (c) ARM and (d) Temperature dependence of κ (up to 700°C) for four representative samples.

Fig. 4: AF (alternating field) demagnetization behavior for 8 representative samples from Hole 709. For the vector component diagrams, open (closed) symbols represent projections onto the vertical (horizontal) plane. The stereoplots are equal-area projections, with solid (open) symbols representing points projected onto the lower (upper) hemisphere. The cores were not azimuthally oriented; declinations are reported in the laboratory coordinate system with respect to the split face of the core. Plots were produced using PuffinPlot (Lurcock and Florindo, 2019).

Fig.5: (a) Magnetic polarity zonation (black = normal polarity and white = reverse polarity), (b) downcore variations of ChRM inclination, (c) MAD. Additional samples collected up to a depth of 266.7 mbsf and analysed at the Laboratório de Paleomagnetismo of Universidade de São Paulo, Brasil:

(d) Magnetic polarity zonation (black = normal polarity and white = reverse polarity), (e) downcore variations of ChRM inclination, (f) MAD.

Fig. 6: Age vs. depth plot. Correlation between the polarity recognized at Hole 709C and the GPTS of Pälike et al., 2006 (Chron C12r to Chron C19n) and the geomagnetic polarity time scale of Cande and Kent, 1995 (Chron C20n and Chron C20r). Calcareous nannofossil datums are used to constrain the interpretation**.**

Fig. 7: Adopted biozonation and the position of the main biohorizons are plotted against magnetostratigraphy. Bioevents used as tie points are indicated in bold.

Fig. 8: Abundance pattern of selected taxa expressed as %, plotted against depth (mbsf) and magnetostratigraphy. The *Discoaster* group includes all the recognized species (*D. adamanteus*, *D. barbadiensis*, *D. bifax*. *D. saipanensis*, *D. tanii*, *Discoaster* sp.); the *Sphenolithus* group includes *S. akropodus, S. intercalaris*, *S. kempii*, *S. moriformis*, *S. obtusus*, *S. orphanknollensis, S. perpendicularis, S. predistentus, S. pseudoradians, S. quadrispinatus, S. radians, S. runus, S. spiniger, S. strigosus*, *S. tribulosus*, the *Reticulofenestra* group includes *R. umbilicus, R. samodurovi* and *R. dictyoda*. Red dashed line indicates the hiatus encompassing the Eocene Oligocene transition.

Fig. 9: Abundance pattern of middle Eocene to early Oligocene warm-water, oligotrophic, and eutrophic taxa plotted against depth (mbsf) and

magnetostratigraphy. Dominance and Shannon-Weaner Diversity indices, PC scores with respect to their corresponding nannofossil groups against age and magnetostratigraphy are shown. The pink line indicates the MECO event, the light blue line points to the Cooling C (Villa et al., 2008, 2014) and the light green area indicates the late Eocene to early Oligocene eutrophic conditions.

Fig. 10: Abundance pattern of early to late Oligocene warm, oligotrophic, and eutrophic taxa plotted against depth and biozones (Agnini et al., 2014). The pink line indicates the late Oligocene warming event.

Figure 1

Click here to download Figure Fig. 1.pdf

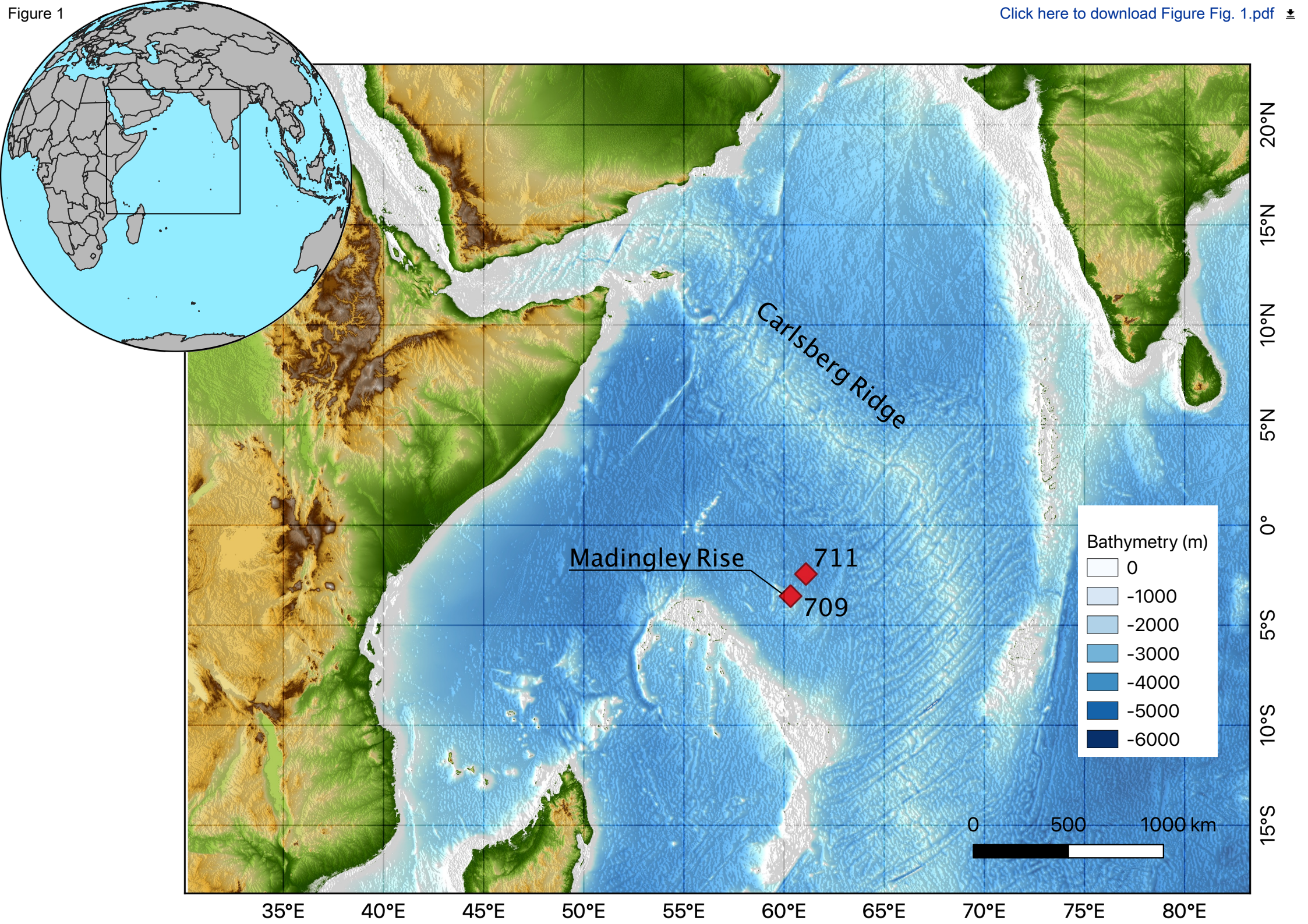

Figure 2

Click here to download Figure Fig. 2.pdf

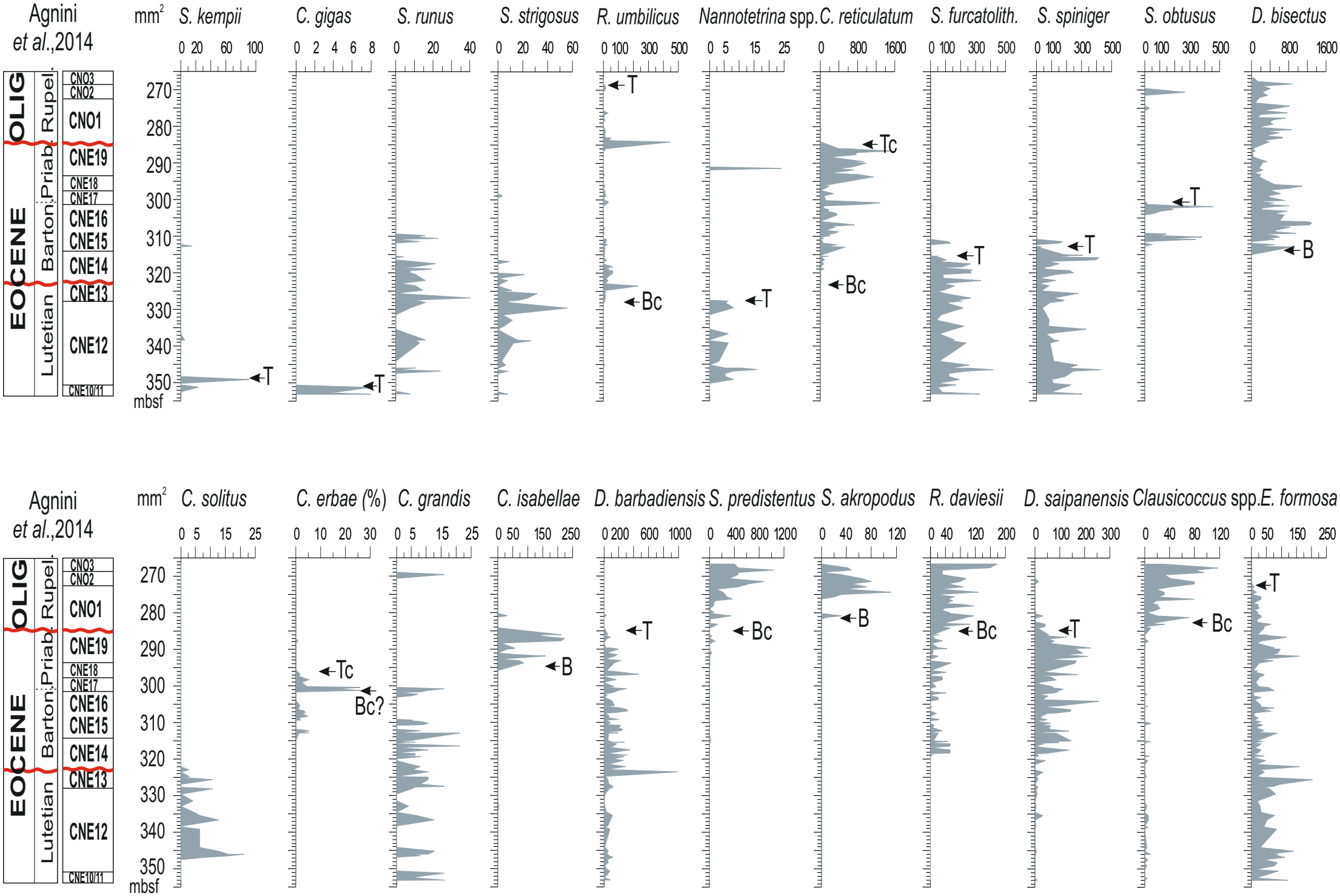

Figure 3

Click here to download Figure Fig. 3.pdf

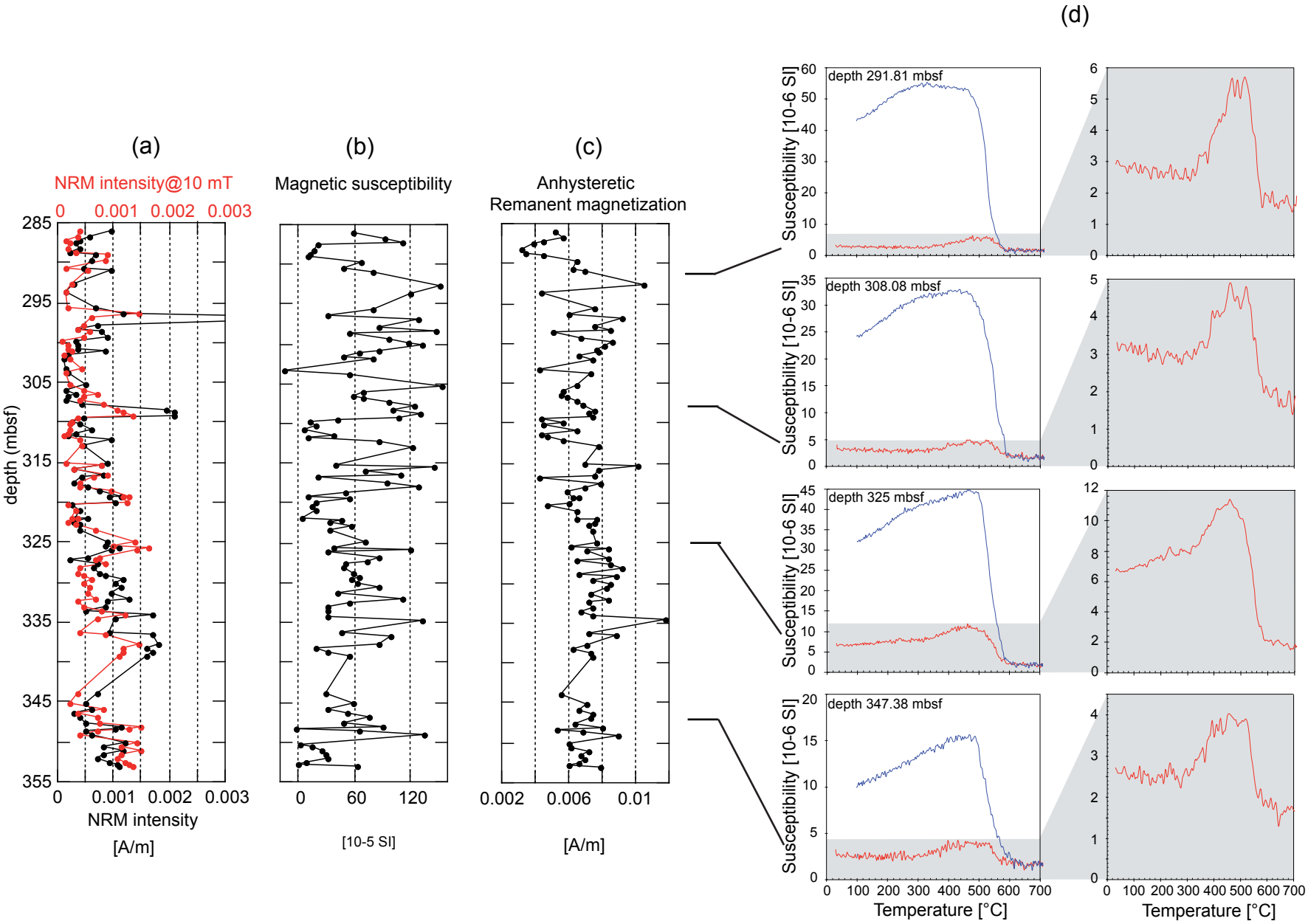

Figure 4

Click here to download Figure Fig. 4.pdf

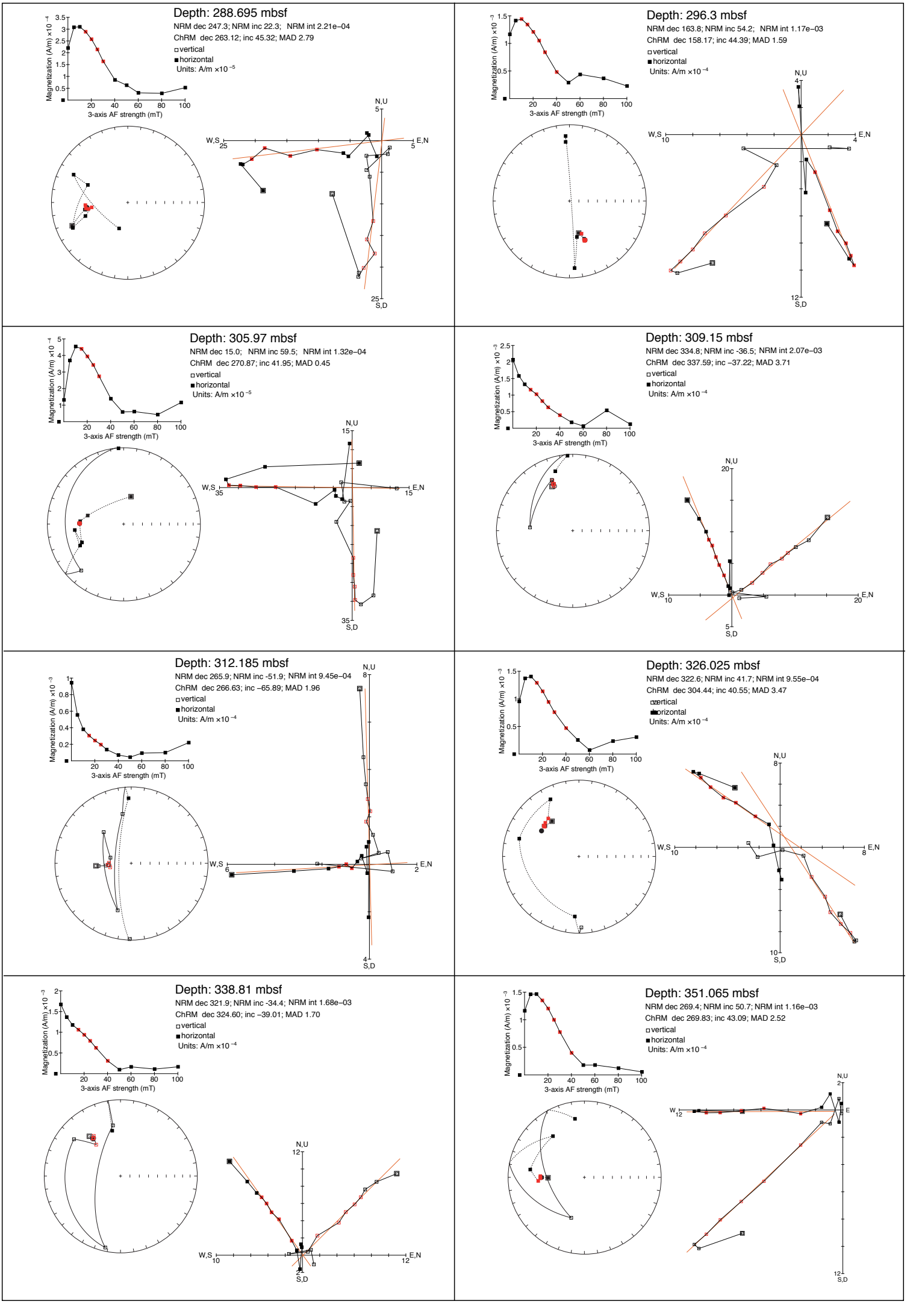

Figure 5

Click here to download Figure Fig. 5.pdf

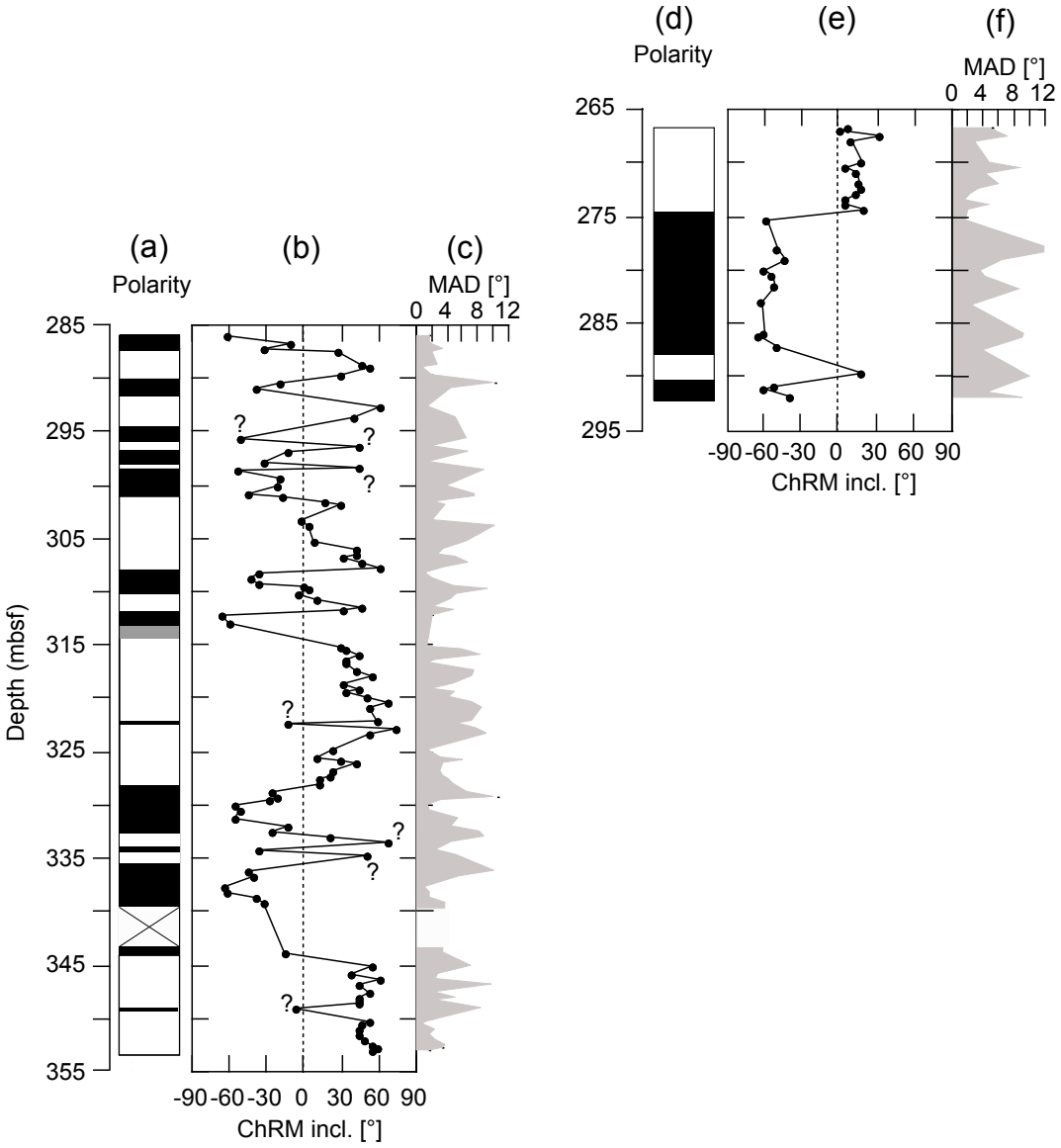

Figure 6

Click here to download Figure Fig. 6.pdf

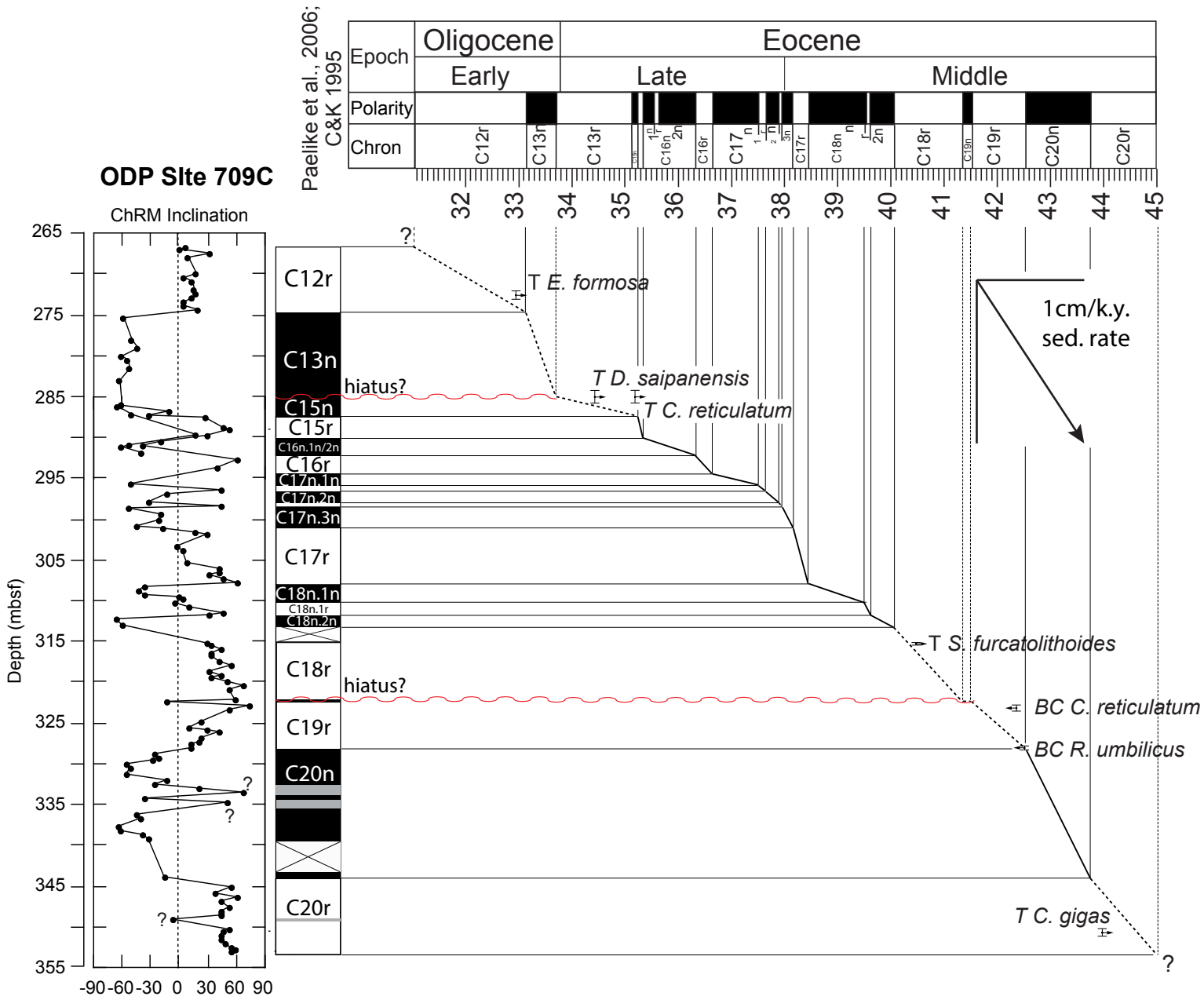

Figure 7

Click here to download Figure Fig. 7.pdf

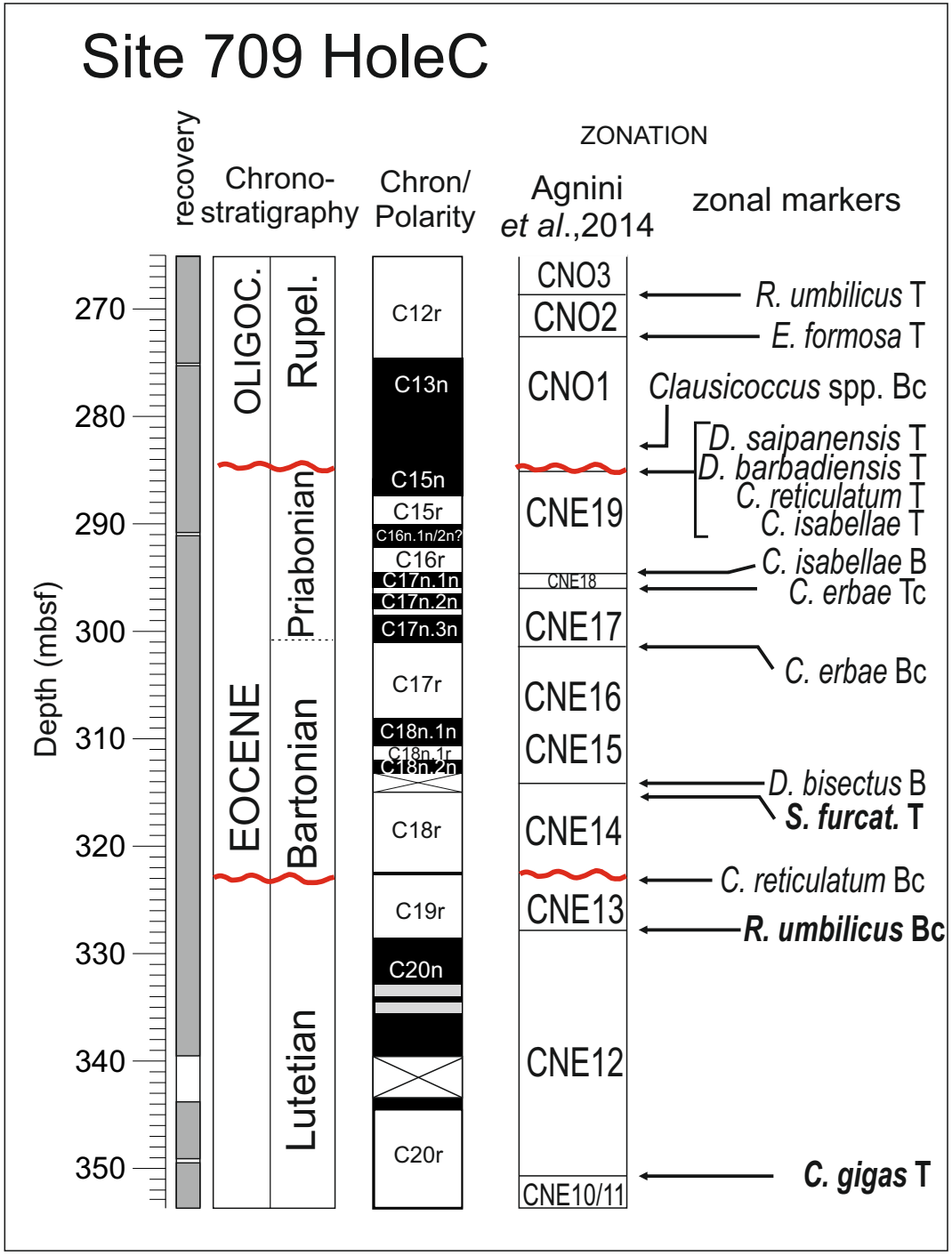

Figure 8

Click here to download Figure FIG. 8.pdf

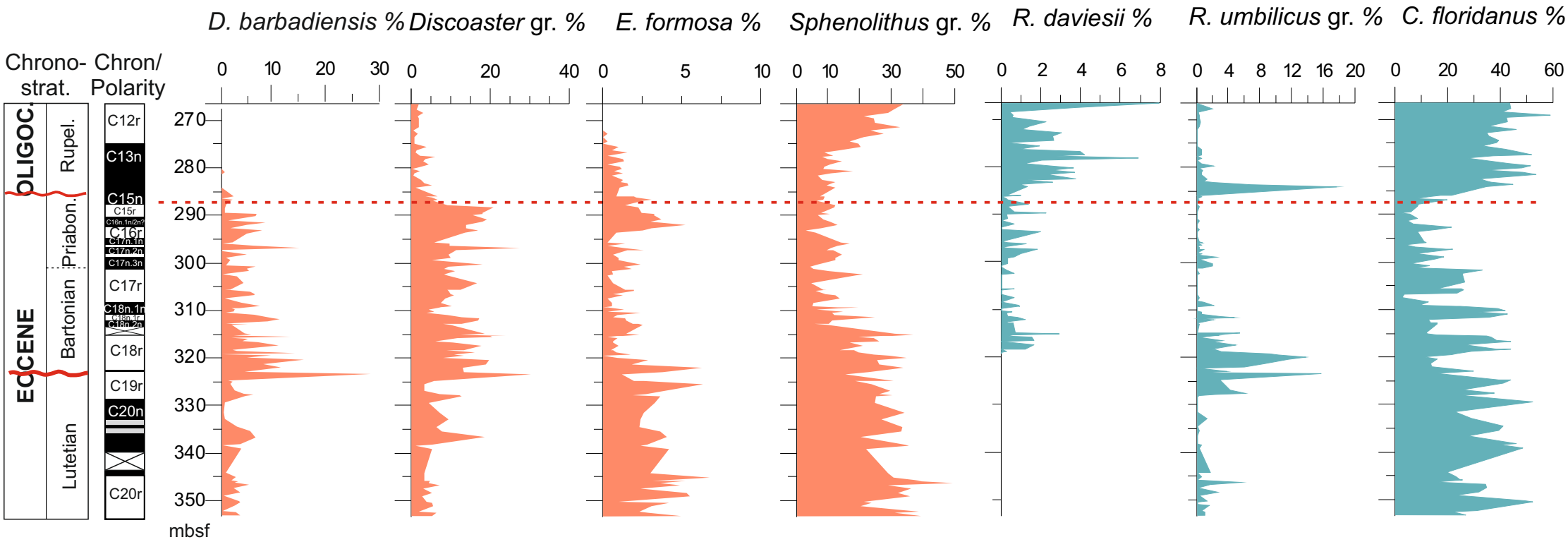

Figure 9

Click here to download Figure Fig. 9.pdf

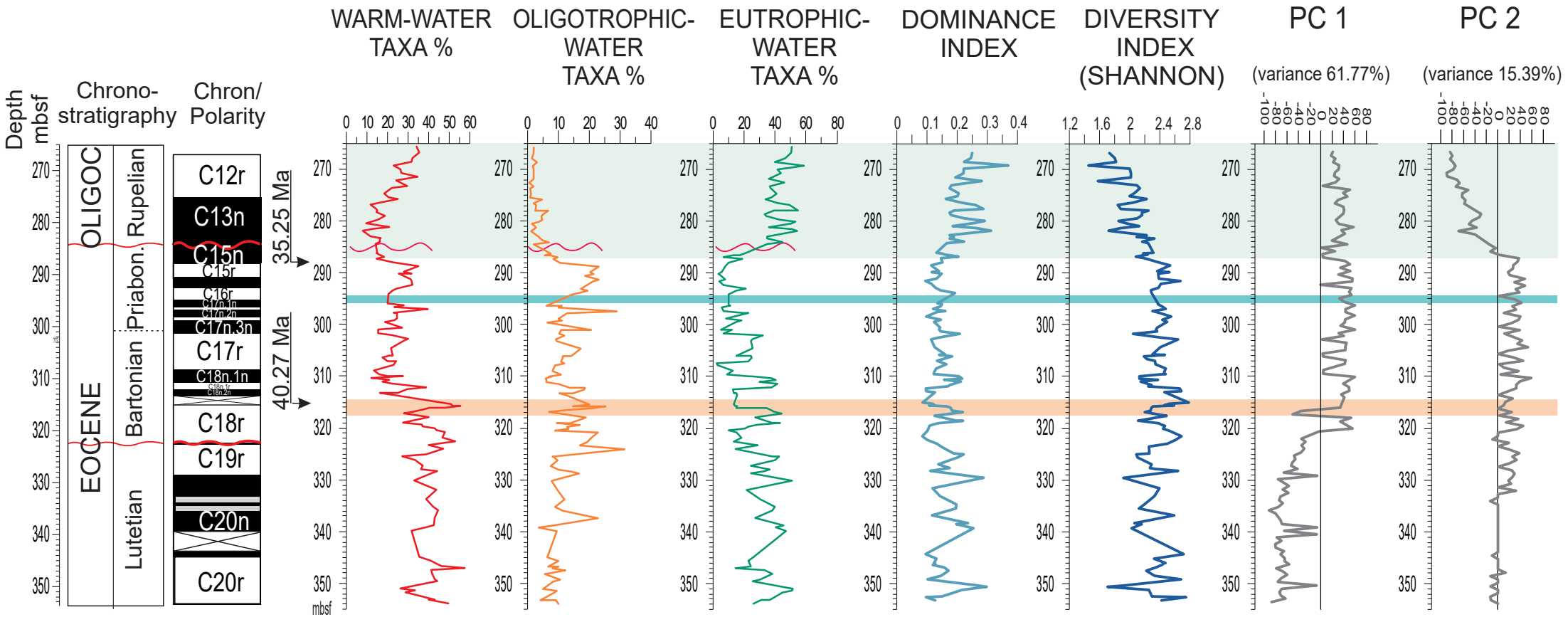

Figure 10

Click here to download Figure Fig. 10.pdf

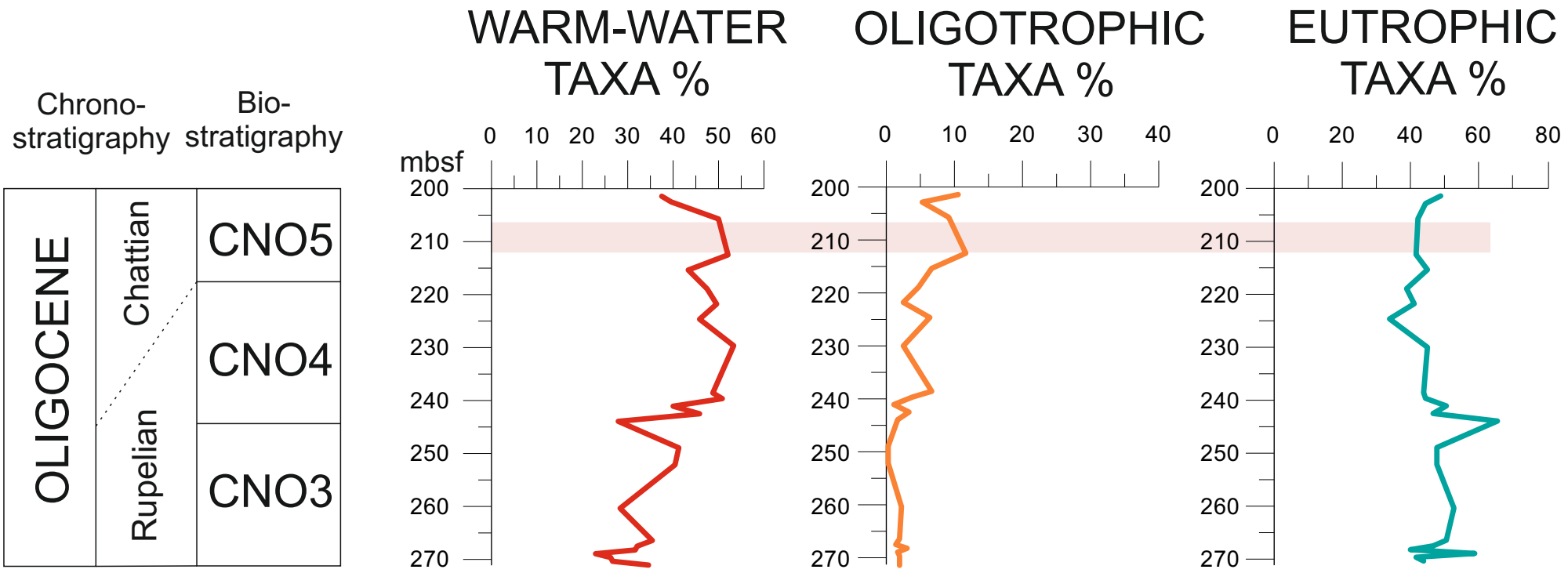

Declaration of interests

☒ The authors declare that they have no known competing financial interests or personal relationships that could have appeared to influence the work reported in this paper.

☐The authors declare the following financial interests/personal relationships which may be considered as potential competing interests:

Click here to access/download

Supplementary Material

Supp material A Villa et al.xlsx